Journal of Thermal Analysis and Calorimetry
https://doi.org/10.1007/s10973-023-12048-w

Energy, exergy, and economic (3E) analyses of nanoparticle-enriched phase change material in an air–PCM heat exchanger applied for buildings free cooling

Sajjad Safarzadeh[1] · Milad Yousefi[1] · Mahdi Kazemi[1] · Ali Kianifar[1]

Received: 3 January 2023 / Accepted: 15 February 2023

Abstract
Common phase change materials (PCMs) have serious shortages, and the most important one is the low thermal conductivity. This issue makes the phase change process a time-consuming period that decreases the performance of thermal storage units. This paper concentrated on improving energy and exergy performance with the aid of an air–PCM heat exchanger, which could be employed for free cooling of buildings. For the heat exchanger, the PCM of Rubitherm 22 °C high capacity (RT22HC) and the nanoparticles of multi-wall carbon nanotube were employed. The initial charging and discharging experiments showed that due to thermal conductivity enhancement, melting and solidification periods decreased using nano-PCM with three concentrations of 0.1, 0.2, and 0.5 mass% compared to the PCM without nanoparticles. Moreover, the highest exergy and energy efficiencies were obtained for the case of nano-PCM 0.5 mass% during the charging process and the values were 11.03 and 21.33%, respectively. Experiments with nano-PCM 0.5 mass% were accomplished during three continuous days. The results demonstrated that the heat obtained from nano-PCM 0.5 mass% encapsulations varied with weather conditions. In addition, the output energy and exergy rose with sunrise and fell with sunset. Finally, an economic analysis was carried out for cold climate conditions. The results indicated that the whole invested capital expenditures will return in the ninth year of exploitation.

Keywords Encapsulation · Heat exchanger · Energy efficiency · Exergy efficiency · Nano-PCM · Economic

List of symbols

a	Equipment accuracy
C	Specific heat (J kg^{-1} K^{-1}), expected cash flow ($)
C_0	Primary investment cost ($)
C_p	Specific heat of the air (J kg^{-1} K^{-1})
E	Energy (kJ)
Ex	Exergy (kJ)
I	Heater electrical current (A)
L_{sf}	Latent heat of fusion (J kg^{-1})
m	Mass (kg)
$\dot{m}_{air}$	Mass flow rate of the air (kg h^{-1})
n	Period that the overall primary investment of project returns to the investors
P	Power (W)
q	Heat transfer rate (kJ)
r	Discount rate
T	Temperature (K)
u	Uncertainty
V	Heater voltage (Volt)
η	Efficiency

Subscripts

ac	Air conditioner
amb	Ambient
e	Electrical
enc	Energy for discharging process
enh	Energy for charging process
eqp	Equipment
exc	Exergy for discharging process
exh	Exergy for charging process
i	Number of periods of project plant life (years or months)
ic	Input for discharging
ih	Input for charging
h	Heater
out	Output
rep	Repetition

✉ Ali Kianifar
a-kiani@um.ac.ir

[1] Department of Mechanical Engineering, Ferdowsi University of Mashhad, Mashhad, Iran

Published online: 27 March 2023

Abbreviations

COP	Coefficient of performance
CF	Equivalent annual cash flow ($)
IRR	Internal rate of return
LHTES	Latent heat thermal energy storage
MWCNT	Multi-wall carbon nanotube
PCM	Phase change material
NPCM	Nano-phase change material
NPV	Net present value
RT22HC	Rubitherm 22 °C high capacity
SSR	Solid-state relay
TEM	Transmission electron microscopy

Introduction

Global warming and changes in living standards have been leading to an increase in the energy usage of air conditioning systems [1]. The consumption of fossil fuels to eliminate energy shortages causes greenhouse gas emissions. Thermal energy storage (TES) technologies are useful for carbon emissions reduction and energy saving [2]. By comparing the different types of TES, the latent heat TES (LHTES) systems are usually chosen due to their small temperature fluctuation and high storage density [3].

Phase change materials (PCMs) are widely employed in LHTES systems. PCMs are utilized in various fields, including solar applications [4–6], cooling systems [7–9], and free cooling and heating of buildings [10–13] because of their stability and considerable latent heat capacity. PCMs are classified in three various types: organic, inorganic, and eutectics [14, 15]. Paraffin is an organic PCM which extensively used due to its suitable thermophysical properties like large latent heat, low cost, non-corrosiveness, and non-toxicity [7, 16]. These properties make paraffins appropriate for use in free cooling and heating of buildings. However, the low thermal conductivity of PCMs is a major problem that reduces their effectiveness in LHTES applications. This problem can be largely solved using nanoparticles [17–19]. Mishra et al. [17] experimentally studied the effect of adding carbon black nanoparticles (CBNP) to a lauric acid-based PCM. They reported a maximum enhancement of about 195% in thermal conductivity by adding 3.5 mass% CBNP to the PCM. Also in another experimental research, Kabeel et al. [18] added graphene oxide nanoparticles to the PCM to improve water production in a solar still. Their results showed a 52% increase in the thermal conductivity of NPCM with respect to pure PCM.

Recently, the application of PCMs in air conditioning (AC) technologies has become an interesting topic for researchers [20–24]. PCMs, which can be used in building structures, release heat during night-time (solidification) and then absorb heat during day-time (melting) in summer due to high temperature variation. Also, PCMs can absorb solar radiation in sunny hours of winter (melting) and use for heating applications. Indeed, to satisfy the thermal comfort in free cooling and heating applications, the suitable temperature range of PCMs for phase transition is from 18 to 30 °C [25].

The energy and exergy analysis is needed to further investigate the thermal performance of the LHTES technologies. The first law of thermodynamics is used in energy analysis, which only considers the energy quantitatively. In contrast, the second law of thermodynamics is needed to evaluate the quality and quantity of energy, i.e., exergy analysis [1]. The irreversibilities are considered in exergy analysis which lead to improvement in the LHTES systems efficiency. Many studies have examined LHTES systems from an energy perspective, but a few investigations have been carried out on exergy analysis of these systems [1, 2, 26–34].

Yadav and Sahoo [29] experimentally studied the exergy and energy efficiency of a LHTES system driven by engine exhaust gas. They conducted exergy and energy analysis for different mass fractions of organic PCMs, including paraffin wax, stearic acid, and lauric acid. Their results at higher mass fractions showed higher exergy and energy efficiency for lauric acid than other two organic PCMs. Nikkerdar et al. [28] numerically evaluated the thermal performance of a PCM–air heat exchanger integrated with a solar air heater. In their study, the tested paraffin (RT25HC) was used as a PCM for a free heating system in a moderate climate condition. They performed exergy and energy analysis for various air channel densities and design temperatures. According to their results, the maximum exergy and energy efficiency is obtained for the 110×110 air channels number. Thermal performance evaluation of a LHTES system using multiple PCMs for free cooling was studied numerically by Mosaffa et al. [30]. They studied the effect of parameters like volumetric flow rate and inlet temperature of air on the exergy efficiency of the system. Based on their results in the charging process, as the inlet temperature decreases from 36 to 32 °C, the exergy efficiency enhances by 6.2%. However, as the volumetric flow rate varies from 800 to 1600 m^3/h, the exergy efficiency increases only by 5.6%. Therefore, the effect of inlet temperature reduction is higher than the volumetric flow rate increasing. Nie et al. [31] experimentally studied the charging performance of a LHTES system using dynamic exergy analysis. They calculated energy and exergy efficiencies for an AC system in various inlet air temperatures and velocities. They reported that maximum exergy efficiency increases with increase in inlet air temperature. Dastmalchi and Boyaghchi [2] numerically investigated the exergy and energy analysis of a PCM–air heat exchanger enriched with nanoparticles for free cooling of buildings. The influence of various slab lengths and PCM thicknesses

was investigated, while the nanoparticles volume fraction was varied from 0 to 5%. Their results showed that maximum exergy efficiency enhancement is 4.1% for the volume fraction of 5%. Tyagi et al. [34] evaluated the thermal performance of a thermal management system (TMS) filled with encapsulated PCM ($CaCl_2{\cdot}6H_2O$) for building cooling. The heating loads of 1–3 kW were selected for discharging process of TMS with an AC system. According to their results, the heating load of 1 kW has the highest energy and exergy efficiencies, while the heating load of 3 kW has the lowest ones. In another experimental study, Tyagi et al. [1] studied two types of PCM-based TMS systems from an energy and exergy perspective for space heating and cooling applications. They used calcium chloride hexahydrate ($CaCl_2.6H_2O$) as the PCM in the climate condition of India. They concluded that exergy efficiency is always less than energy efficiency for both types of TMS systems during the heating and cooling process.

This article intends to experimentally study the thermal performance of a PCM–air heat exchanger dispersed with multi-wall carbon nanotubes (MWCNTs). To the authors' best knowledge, the investigation of energy and exergy analyses in building free cooling and heating applications has been rarely studied. In this work, the influence of various inlet temperatures and nanoparticle concentrations on energy and exergy efficiencies of a PCM–air heat exchanger during heating and cooling periods are studied. Moreover, the variations of outlet energy and exergy of the heat exchanger during three successive days are evaluated. Finally, an economic analysis is conducted for cold climate conditions.

Experimental

Materials and properties

At a nearly constant temperature, to release and store a noticeable amount of thermal energy, PCMs are employed for the processes of congealing and melting. To this end, the PCM of RT22HC (Rubitherm 22 °C High Capacity), with the features of non-toxicity and high capacity is purchased. According to the local weather condition, the selected PCM has a melting temperature range of 20–23 °C. The PCM thermo-physical properties are indicated in Table 1. Some of them are specific heat capacity, thermal conductivity, and density. Figure 1 indicates the DSC curves of paraffin and nano-PCMs of 0.2 and 0.5 mass%, presented in our previous study [35]. The first peak, which is not fully revealed due to the minimum temperature in the DSC test, happens because of the solid–solid phase transition. The second peak (exothermic) shows the solid–liquid phase transition.

The addition of nanoparticles of MWCNT to the PCM is recommended because of the PCM's low thermal conductivity [35, 36]. Employing NPCM in the free cooling field is one of the purposes of this study. Due to nanoparticles agglomeration, dispersing nanoparticles in PCM is a significant issue. Using functionalized nanoparticles can solve this problem. So, MWCNT with carboxyl functional group (MWCNT-COOH) is considered as the selected nanoparticle due to its high thermal conductivity (as presented in Table 2, US Research Nanomaterials Inc.). A group of hydroxyl (O–H) is attached to the atom of carbon of a carbonyl group (C=O) and makes the carboxyl group (COOH) called a functional group. Figure 2 indicates the MWCNTs TEM image [35]. The carboxyl group in these nano-sized powders helps the particles better dispersing in the PCM. Thus, MWCNT-COOH nanoparticles are selected in the process of NPCM construction. A specific mass fraction of

Table 1 Thermophysical properties of PCM presented by the manufacturer [37]

Thermal properties	Value
Melting range	20–23 (°C)
Heat storage capacity	190,000 (J kg^{-1})
Heat conductivity (both phases)	0.2 (W m^{-1} K^{-1})
Specific heat capacity	2000 (J kg^{-1} K^{-1})
Density in solid state at 20 °C	0.76 (kg l^{-1})
Density in liquid state at 50 °C	0.7 (kg l^{-1})
Volume expansion	12.5 (%)
Flash point	> 150 (°C)

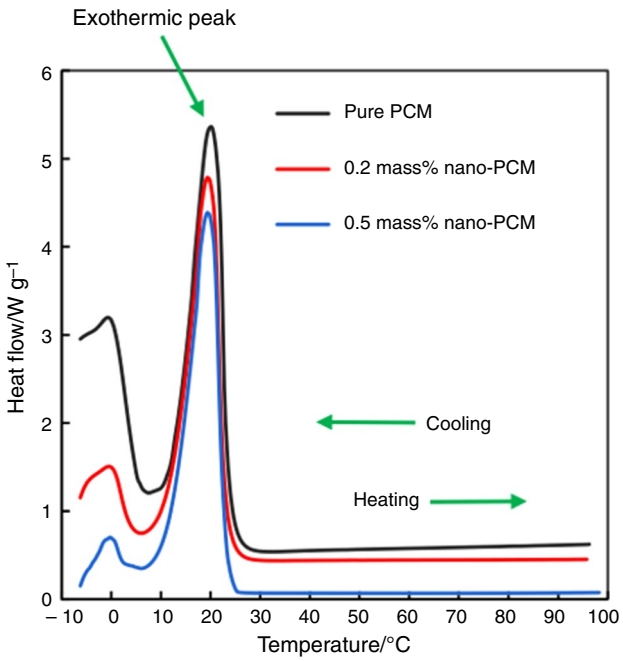

Fig. 1 DSC curves of the PCM and nano-PCMs [35]

Table 2 Nanoparticle features (MWCNT-COOH) [36]

Nanoparticle features	
Functional group	Carboxyl
Purity	95%
Diameter/nm	20–30
Length/μm	5–10
Effective area/m^2 g^{-1}	> 200
Apparent density/g cm^{-3}	2.1

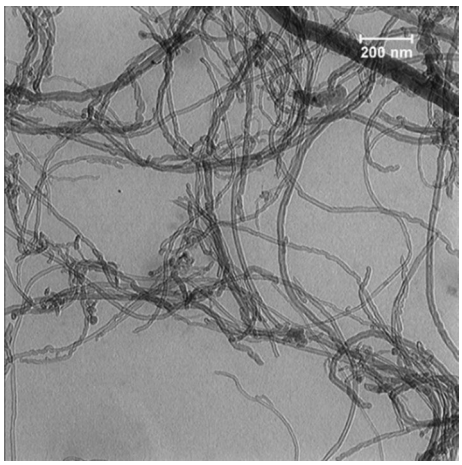

Fig. 2 An image of TEM related to MWCNT-COOH nanoparticles [35]

nanoparticles is added to the PCM. Then, obtained mixture is stirred at 30 °C and a speed of 100 rpm. Next, an ultrasonic bath (Elma, Elmasonic, S60H, and Germany, with 400 watts power and 37 kHz frequency) is employed to put the mixture inside. The bath temperature and sonication time would be 40 °C and 30 min, respectively. Finally, a stable NPCM is achieved. For the present study, four different mass fractions are considered (0%, 0.1%, 0.2%, and 0.5%).

The thermal conductivity and latent heat of fusion for both liquid and solid phases were measured in our previous paper [35]. It concentrated on evaluating the PCM and NPCM during solidification and melting periods. Table 3 shows these parameters for PCM and NPCMs.

Experimental setup

3D and 2D schematic views of the experimental apparatus are displayed in Fig. 3a and b, respectively. A fan with an axial type is used to move the air through the heat exchanger (in an open-air circuit). Providing a constant temperature air is the duty of cooling and heating unit devices. Cooling and heating units are included a compression refrigeration cycle and heater elements, in order. As shown in Fig. 3, for the thermal energy storage part, a shell-and-tube heat exchanger is examined. To track the influence of changes in temperatures of air and PCMs, the tubes are made of aluminum and have flat plate closures. The closures contain PCM inside and are called PCM encapsulations. Each encapsulation is fabricated with dimensions of $15 \times 15 \times 2$ cm. Besides, dimensions of $65 \times 18 \times 25$ cm are considered for the shell, which is a container. Furthermore, the shell is fabricated by wooden plates (with a thickness of 1.5 cm), and to minimize thermal losses, it is covered by elastomeric insulation.

To set the air inlet temperature to a specific value, a control temperature system is used, which is automatic. The control system comprises a TC4Y temperature indicator and an SSR (solid-state relay) connected to the cooling and heating unit. Whenever the inlet thermocouple wants to raise the temperature (for example, 27 °C), the SSR receives a signal from the indicator, and the heater power is controlled by the electric current, and desired temperature is provided.

The encapsulations which contain PCM are placed parallel to the flow of air such that the flow of air can move along the PCM encapsulations. Between each two of them, a 20-mm gap is considered. It must be noted that the temperature of PCM is measured just for one encapsulation due to the symmetry and excellent insulation, as stated in our previous research [36]. Thus, the inlet, outlet, and PCMs temperatures are measured and saved utilizing five calibrated thermocouples with the type of DS18B20. In addition, to measure the airflow velocity, a calibrated UT211B 60A Mini Clamp Meter is used.

Uncertainty investigation

Uncertainty investigation demonstrates how the input parameters' uncertainty of a mathematical model affects the variable of output and evaluates the reliability of the

Table 3 Thermal conductivity and latent heat of fusion in both solid and liquid phases [35]

Samples	Thermal conductivity (solid phase)/W m^{-1} K^{-1}	Thermal conductivity (liquid phase)/W m^{-1} K^{-1}	Latent heat of fusion/kJ kg^{-1}
Pure PCM	0.136	0.132	210
NPCM 0.2 mass% MWCNT	0.184	0.157	184.3
NPCM 0.5 mass% MWCNT	0.203	0.192	180.1

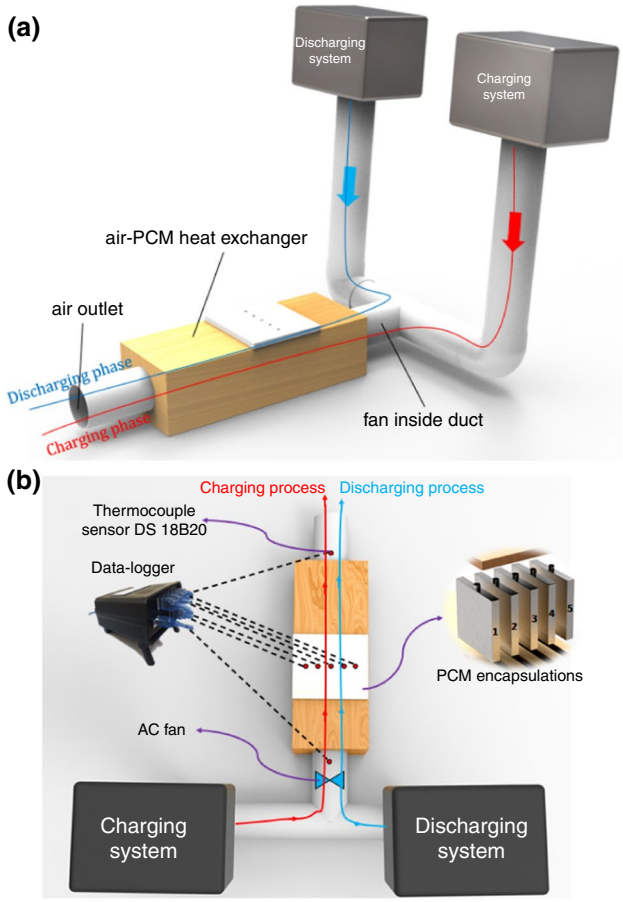

Fig. 3 **a** 3D and **b** 2D schematic views of the experimental setup included heat exchanger and PCM encapsulations

results. However, uncertainty analysis is applied based on the method proposed in Ref. [38]. Equation (1) calculates the total uncertainty for each parameter according to the uncertainty of repetition (δu_{rep}) and uncertainty of equipment (δu_{eqp}) [38].

$$\delta u = \sqrt{(\delta u_{rep})^2 + (\delta u_{eqp})^2} \tag{1}$$

The repetition uncertainty (δu_{rep}) and uncertainty of equipment (δu_{eqp}) are presented by the following equations:

$$\delta u_{eqp} = \frac{a}{\sqrt{3}} \tag{2}$$

$$\delta u_{rep} = \frac{\sigma}{\sqrt{N}} \tag{3}$$

In Eq. (2), half of the equipment accuracy is expressed by a. In Eq. (3), the parameter N and σ are the numbers of the repeated measured data and the standard deviation, in order.

Considering G to be a function of 'n' linear parameters which are independent, ∂G, δu_i, and $\partial G/\partial u_i$ are defined as the function G uncertainty, the u_i uncertainty, and the partial derivative of G, in order [38]. Thus, Eq. (4) is the uncertainty of the function G:

$$\partial G = \sqrt{\left(\frac{\partial G}{\partial u_1}\delta u_1\right)^2 + \left(\frac{\partial G}{\partial u_2}\delta u_2\right)^2 + \ldots + \left(\frac{\partial G}{\partial u_n}\delta u_n\right)^2} \tag{4}$$

Table 4 shows the accuracy and the repetition, equipment, and total uncertainty for each measuring equipment. This analysis ascertains the high reliability of experimental results since the uncertainty is less than 3%.

Measurements

Energy analysis

The equations used in the energy analysis of the PCM–air heat exchanger system can be given as follows:

For the storage process, the energy balance is written as below [34]:

Energy input − [energy loss energy + recovered] = accumulation of energy.

Output energy can be given as [39–41]:

$$E_{out} = m_{PCM}C_{PCM}\left(T_{end} - T_{start}\right) + m_{PCM}L_{sf} \tag{5}$$

where m_{PCM} is the mass of the PCM, C_{PCM} is the specific heat capacity of the PCM, T_{end} and T_{start} are the final and initial temperatures of the PCM, respectively, and L_{sf} is the latent heat of melting.

The energy input for the charging process is written as below:

Table 4 Uncertainty of measuring parameters

Equipment	Measurement section	Accuracy	u_{eqp}	u_{rep}	u_{tot}
DS18B20 thermocouple	Inlet/outlet temperature	±0.2 °C	0.058	0.099	0.115 °C
DS18B20 thermocouple	Ambient temperature	±0.2 °C	0.058	0.170	0.180 °C
DS18B20 thermocouple	Encapsulation temperature	±0.2 °C	0.058	0.047	0.075 °C
UT211B clamp, flow meter	Air velocity	±(0.8% + 2) m s^{-1}	0.017	0.086	0.087 m s^{-1}
Ruler	Geometries	1 mm	0.289	0.047	0.292 mm

$$E_{ih} = P_h \tag{6}$$

where P_h is the power of the electric heater and can be calculated using Eq. (7):

$$P_h = V \times I \tag{7}$$

where V and I are the heater voltage and electrical current, in order.

The energy input for the discharging process is written like so:

$$E_{ic} = P_{ac} \tag{8}$$

where P_{ac} is the power of the air conditioner.

Also, when the air flows through encapsulations, the heat transfer rate can be given as follows:

$$q_{air} = \dot{m}_{air} C_p (T_{in} - T_{out}) \tag{9}$$

where $\dot{m}_{air}$ is the mass flow rate of the air, C_p is the specific heat capacity of the air, and T_{in} and T_{out} are the inlet and outlet temperatures of the air, respectively.

To better evaluate and compare the PCM–air heat exchanger from an energy perspective, a parameter called energy efficiency is introduced. This efficiency is determined as the output energy ratio which is absorbed/released by PCM to input energy and can be given as [42–46]:

$$\eta_{energy} = \frac{\text{Energy(output)}}{\text{Energy(input)}} \tag{10}$$

For the charging process, the energy efficiency is written using Eq. (11):

$$\eta_{enh} = \frac{E_{out}}{E_{ih}} \tag{11}$$

Energy efficiency for the discharging process is written as below:

$$\eta_{enc} = \frac{E_{out}}{E_{ic}} \tag{12}$$

Exergy analysis

The exergy balance for the storage process can be given utilizing following relation:

Exergy input − [exergy recovered + exergy loss] − energy consumption = exergy accumulation.

The below equation is proposed for output exergy [42–46]:

$$\begin{aligned} \text{Ex}_{out} = \; & m_{PCM} C_{PCM} (T_{end} - T_{start}) \\ & + m_{PCM} L_{sf} (1 - T_{amb}/T_{source}) \\ & - m_{PCM} T_{amb} C_{PCM} \cdot \ln (T_{end}/T_{start}) \end{aligned} \tag{13}$$

where m_{PCM} is the mass of the PCM, C_{PCM} is the specific heat capacity of the PCM, T_{end} and T_{start} are the final and initial temperatures of the PCM, respectively, L_{sf} is the latent heat of melting PCM, T_{amb} is the ambient temperature and T_{source} is the temperature of the charging/discharging source.

Furthermore, the exergy input for the charging process is written as below:

$$\text{Ex}_{ih} = P_h \times \eta_e \tag{14}$$

where η_e is the efficiency of the electric heater.

The exergy input for the discharging process is written as:

$$\text{Ex}_{ic} = P_{ac} \times \text{COP} \tag{15}$$

where COP is the coefficient of performance of the air conditioner.

Like energy analysis, a parameter called exergy efficiency for this system is introduced. The exergy efficiency is determined as the output exergy to input exergy ratio and can be given as follows [42–46]:

$$\eta_{exergy} = \frac{\text{Exergy(output)}}{\text{Exergy(input)}} \tag{16}$$

Exergy efficiency for the charging and discharging processes is:

$$\eta_{exh} = \frac{\text{Ex}_{out}}{\text{Ex}_{ih}} \tag{17}$$

$$\eta_{exc} = \frac{\text{Ex}_{out}}{\text{Ex}_{ic}} \tag{18}$$

Results and discussion

Effect of nanoparticles concentration

As observed in Fig. 4, due to different heat transfer modes and storage mechanisms like conduction and convection heat transfer, sensible heating, and latent heating phenomenon, the effect of the mass fraction of PCM on the transient encapsulation temperature doesn't have a linear trend. For the system response, six stages are considered. The first stage of the system, where a sharp rise in temperature curve is observed, is defined as sensible heating without melting. As the melting process begins, stage two begins. The slope of temperature declines in this stage. Moreover, sensible heating in the post-melting stage appears as a melting period

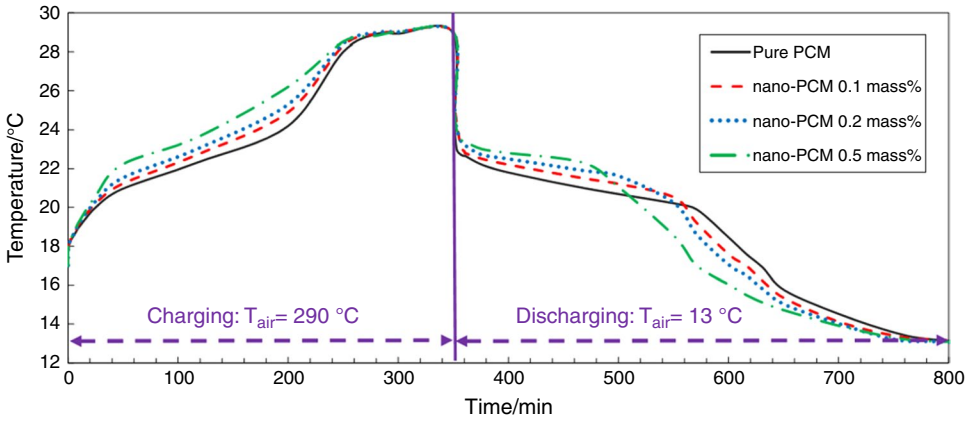

Fig. 4 Temperature evolution vs. time for the pure PCM and NPCM (3 concentrations) during charging (inlet temperature of 29 °C) and discharging (inlet temperature of 13 °C) periods

of NPCM or pure PCM finishes. Next, a steady-state condition (29 °C) is observed by a monotonic increase in the temperature of the encapsulation. Besides, for the encapsulation cooling period, a similar analysis can be defined. The fourth stage is sensible cooling. In the next period, a change in the temperature curve slope starts, and solidification takes place. In the final stage, the encapsulation temperature reduces to 13 °C during the post-sensible cooling. Adding CNTs to the pure PCM provides a more thermal conductor PCM which can absorb/release heat more than the pure one. So, the sixth stage for nano-PCM has a sharper slope.

Furthermore, using the NPCM compared to pure PCM in lab-scale experiments augments the curve slope. This phenomenon indicates the higher melting and solidification rates of the NPCM cases compared to that of the pure PCM, demonstrating an increase in the heat quantity charged into/discharged from the encapsulations per unit of time.

Figure 5a displays the variation of energy efficiency of the PCM–air heat exchanger during the charging period for pure PCM and NPCMs of 0.1, 0.2, and 0.5 mass%. Three different temperatures are considered for the inlet temperature of the heat exchanger: 25, 27, and 29 °C. For all PCM cases, the energy efficiency is enhanced as inlet air temperature increases. This increase in the case of NPCM 0.5 mass% is nearly 20% when the inlet temperature varies from 25 to 29 °C. Nevertheless, at a constant temperature of 29 °C, the addition of MWCNT of 0.1, 0.2, and 0.5 mass% to the pure PCM would improve the energy efficiency by approximately 3.7, 5.6, and 7.7%, respectively. The maximum energy efficiency of 21.33% is devoted to NPCM 0.5 mass% and the inlet air temperature of 29 °C.

Figure 5b displays the variation of energy efficiency of pure PCM and NPCMs of 0.1, 0.2, and 0.5 mass% during the discharging period. The energy efficiency is obtained for the inlet air temperatures of 13, 15, and 17 °C. It is seen from Fig. 5b that temperature reduction of the inlet air raises energy efficiency. Moreover, the charging energy efficiency is greater than that of the discharging phase due to the slowness of discharging period. Furthermore, at the inlet air temperature of 13 °C, the maximum energy efficiency is calculated for the case of NPCM 0.5 mass%, which is nearly 11.44%.

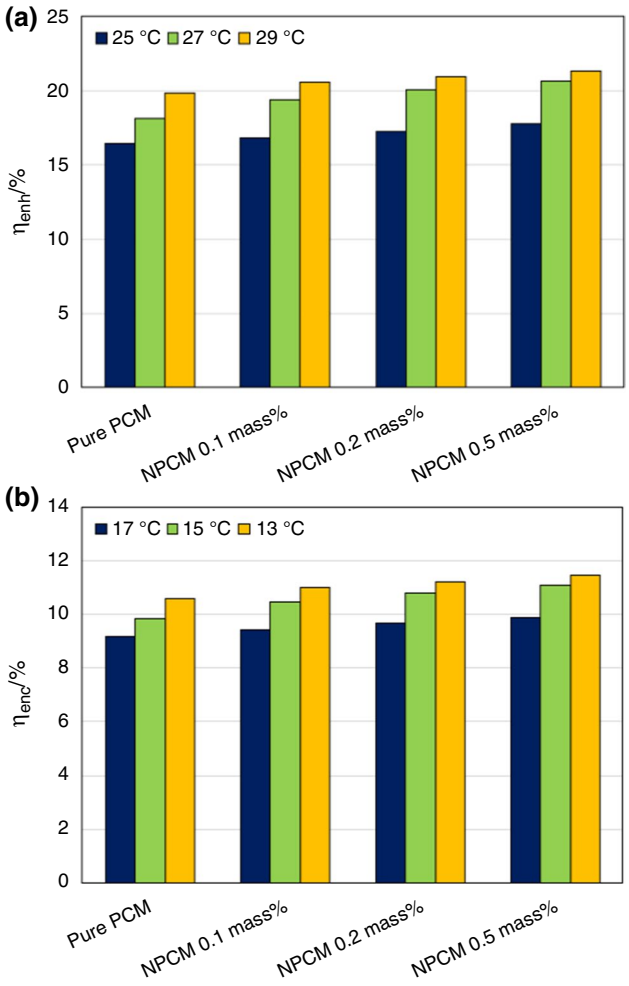

Fig. 5 Energy efficiency of pure PCM and NPCM of 0.1, 0.2, and 0.5 mass% during **a** charging and **b** discharging periods

The variation of exergy efficiency of the PCM–air heat exchanger during the charging process for pure PCM and NPCMs 0.1, 0.2, and 0.5 mass% is shown in Fig. 6a. The exergy efficiency is calculated at temperatures of between 25 to 29 °C. Considering the pure PCM, increasing the inlet air temperature improves the exergy efficiency, similar to the energy efficiency. This increase equals about 2% for changing the air inlet temperature from 25 to 29 °C. However, at a constant temperature such as 25 °C, the addition of carbon nanoparticles of 0.1, 0.2, and 0.5 mass% only increases the exergy efficiency by 0.21, 0.44, and 0.66%, respectively. Therefore, the results show the importance of the inlet air temperature on the exergy efficiency of the PCM–air heat exchanger. For each inlet temperature, the NPCM 0.5 mass% has the highest exergy efficiency. This is attributed to the fact that according to Table 3, the thermal conductivity of both liquid and solid phases of PCM increases by nanoparticle addition, which leads to an increase in the PCM temperature and exergy efficiency. Moreover, the specific heat of NPCM increases due to adding nanoparticles, which results from the interaction between MWCNT and pure PCM. The maximum exergy efficiency is obtained for NPCM 0.5 mass% and the inlet air temperature of 29 °C, which is equal to 11.03%.

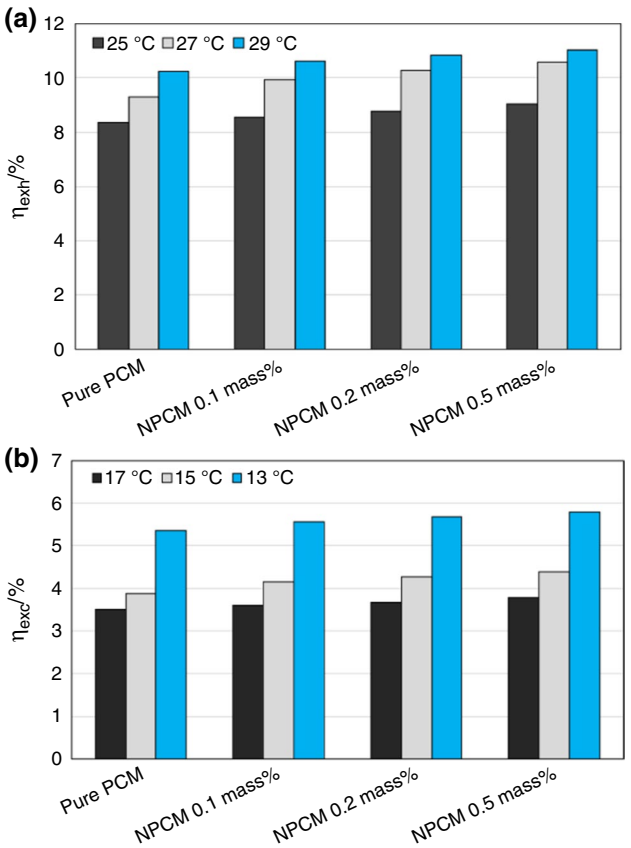

Fig. 6 Exergy efficiency of pure PCM and NPCM of 0.1, 0.2, and 0.5 mass% during **a** charging and **b** discharging periods

The variation of exergy efficiency during discharging process for pure PCM and NPCMs 0.1, 0.2, and 0.5 mass% is depicted in Fig. 6b. The exergy efficiency is obtained for the temperature range of 13–17 °C. Similar to the energy efficiency, it is concluded that the exergy efficiency increases with decrease in the inlet air temperature. As mentioned earlier, due to the slowness of discharging process, the exergy efficiency values of discharging period are lower than the charging process. Also, the maximum exergy efficiency is calculated for NPCM 0.5 mass% and the inlet air temperature of 13 °C, which is equal to 5.8%.

From energy and exergy efficiency diagrams, it is deduced that the exergy efficiency is always lower than energy efficiency. This is because the energy efficiency is computed from the first law of thermodynamics. The first law describes the quantity of energy but does not discuss the losses/irreversibility. However, the exergy efficiency is obtained using the second law of thermodynamics which describes the quality of energy and considers the losses/irreversibilities.

This part evaluated the pure PCM and NPCMs 0.1, 0.2, and 0.5 mass% based on temperatures, and energy and exergy efficiencies to determine which case is the best. According to obtained results, the NPCM 0.5 mass% has the best (highest) efficiency among other cases. Therefore, this case is selected for the outdoor experiments.

Another way to use phase change materials in buildings free cooling is to prepare PCM panels and put them in the wall to control room temperature. Tyagi et al. [34] employed PCM of $CaCl_2{\cdot}6H_2O$ with the latent heat of 140 kJ/kg and melting temperature of 24 °C for their thermal management system (TMS). A schematic of this study is displayed in Fig. 7.

By comparing both studies from Fig. 8, it is shown that the current system has a noticeable efficiency (energy, exergy, and total) compared to that proposed by Tyagi et al. [34] for the charging period. It means that the total efficiency for TMS and NPCM 0.5 mass% is 7.1 and 30.1%, respectively, indicating a nearly 312% improvement. This noticeable enhancement is not observed for discharging period. The TMS has a total efficiency of 14.7%. This parameter for the current study with pure PCM and NPCM 0.5 mass% is 14.2 and 15.5%, in order, which shows almost the equality of both systems in the discharging process. Moreover, as observed in Fig. 8 (discharging), the current heat exchanger can compete with the TMS from an energy viewpoint. However, the exergy efficiency of the TMS is much higher that can compensate for its lack of energy efficiency and reach its total efficiency approximately to the other cases.

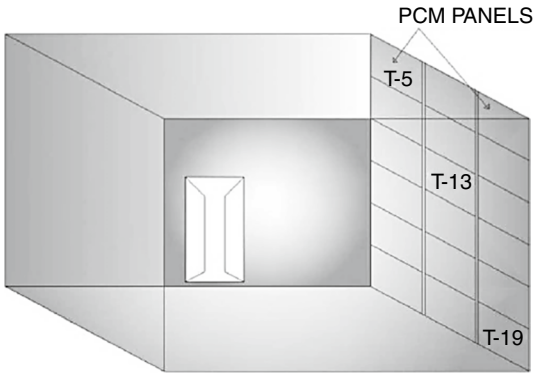

Fig. 7 The TMS schematic using PCM panels inside room wall [34]

Outdoor analysis

Figure 9a illustrates inlet temperature, outlet temperature, and amount of heat charged in or discharged from the encapsulations containing NPCM 0.5 mass% under three consecutive winter days. It should be stated that in this experiment, the ambient air is the inlet fluid. According to this figure, the warm air flows through the encapsulations during the daytime until the encapsulations' temperature reach nearly the inlet temperature. Meanwhile, heat of the air (and maybe the sun) is charged into the encapsulations, and the air temperature drops before entering the building. While night-time, the heating process is vice versa. The encapsulations, which absorb the air (and maybe the sun) heat, release it to the inlet air to raise the air temperature for the building. As it is indicated in Fig. 9a, the three continuous days have an ascending temperature, a maximum temperature of nearly 27.5 °C (day 1) to 30.5 °C (day 3). At day 1, due to lower air temperature, the NPCM misses the third stage. Therefore, the magnitude of heat discharged from the air into the encapsulations is the lowest over the three days.

In this case study, it is observed that the thermal energy obtained or discharged from the NPCM 0.5 mass% encapsulation packs varies with the change in the weather conditions. The maximum heat charged into and discharged from the encapsulations is 67.1 and − 89.6 W, respectively. It should be mentioned that the rapid solidification and melting rates can enhance the amount of heat per unit of time that is discharged from or charged in the encapsulation packs. Besides, it is detected that the slope magnitude of the heat curve using the NPCM 0.5 mass% has higher values when the encapsulations pass the phase-changing zones because, in these zones, the temperature difference between the inlet and outlet is considerable. In addition, as the encapsulations couldn't finish the fifth and sixth stages on day 1, the output energy has a much lower amount (about 17 kJ) over the three days.

Figure 9b displays the variation of the output energy and exergy for the case of NPCM 0.5 mass% during three successive winter days. Based on this figure, both the output energy and exergy are low initially. However, when the time increases, both the energy and exergy increase at a similar trend until the encapsulation temperature reaches to inlet value (at the end of each day). Then, the intensity of sunlight gradually decreases and both values decrease until the next day. This trend repeats consecutively within two next days with higher values for both the output energy and exergy due to energy and exergy storage in the NPCM. This is because of the fact that output energy and exergy are functions of the sensible and latent heat of NPCM. It is also found that the output exergy is always lower than the output energy because the output exergy is calculated via second law of thermodynamics which considers the irreversibilities. The maximum values of output energy and exergy are about 325 and 24 kJ, respectively.

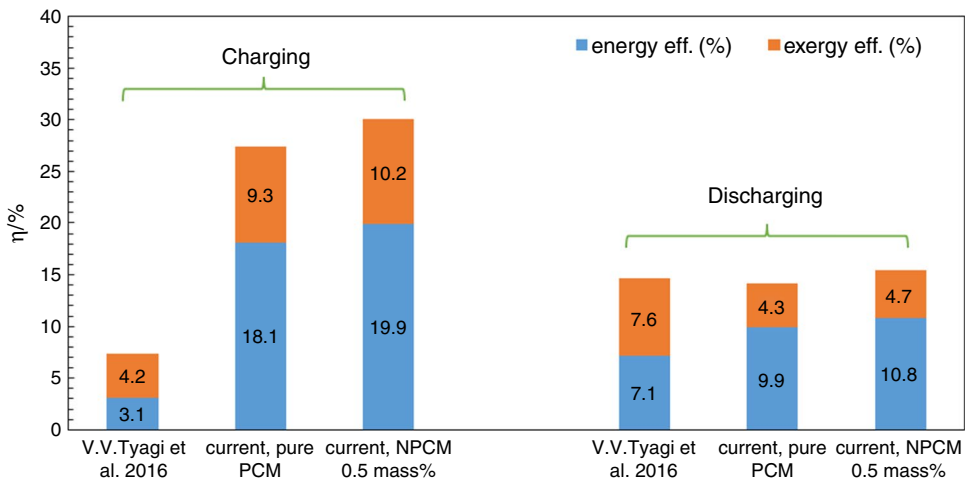

Fig. 8 Energy, exergy, and total efficiency of the TMS [34] and the current heat exchanger with the pure PCM and NPCM 0.5 mass% for the charging and discharging periods

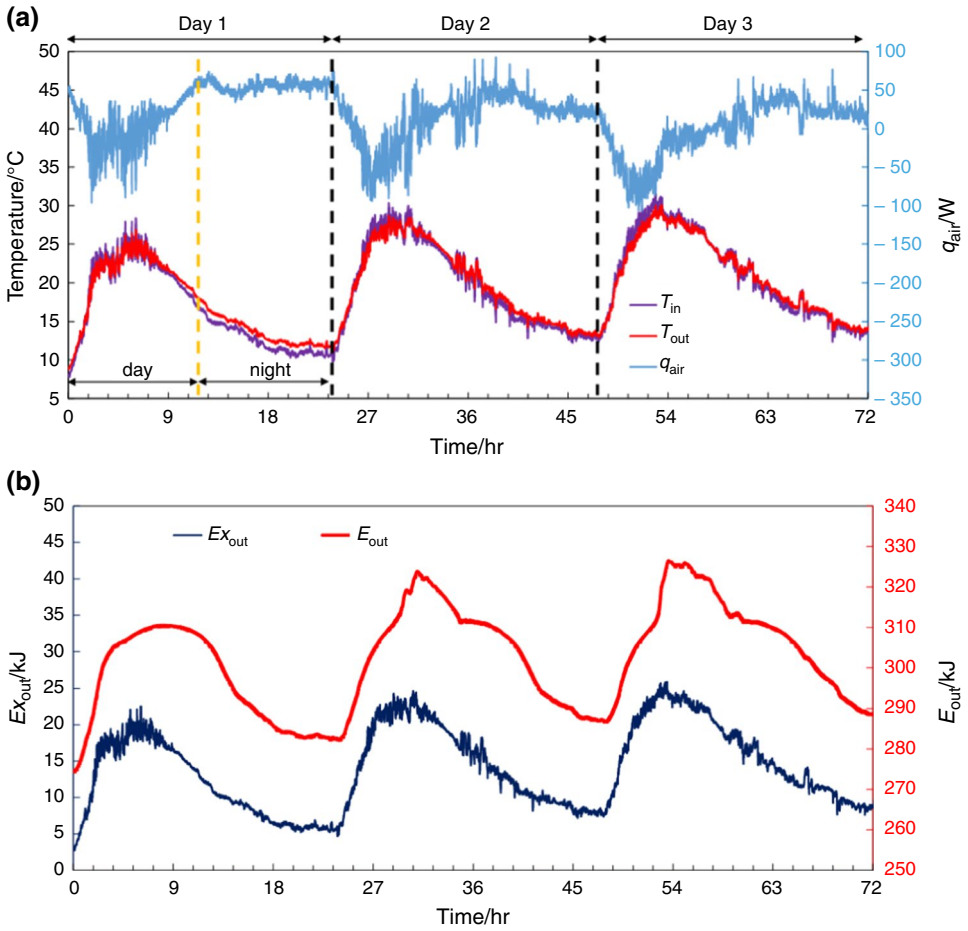

Fig. 9 **a** Inlet temperature, outlet temperature, and amount of heat charged in or discharged from the encapsulations contains NPCM 0.5 mass% under three consecutive winter days, and **b** The variation of the output energy and exergy for the case of NPCM 0.5 mass% under three successive winter days

Table 5 Assumptions of economic assessment for the air–PCM heat exchanger

Parameter	Value
Capital expenditures/$	1400
Operating cost/$	140
Inflation rate/%	7.6
Energy gain/J $year^{-1}$	5.2×10^{7}
Gas consumption saving during a year/$ $year^{-1}$	402.2
Natural gas price/$ 10^{-6} Btu	5.415

Economic analysis

The economic aspect is a significant issue for the final evaluation of specified weather conditions. In the following, for cold climate conditions, an economic analysis of the air–PCM heat exchanger has been accomplished. Table 5 represents the significant assumptions for the economic assessment of the current system.

In this economic investigation, the technique of discounted cash flow (DCF) is employed. Three criteria are defined for this technique utilized for choosing the most profitable and economic project [47].

At first, at the project beginning, the overall incomes obtained in future are converted into the equivalent earnings with an appropriate discount rate. To measure net present value (NPV), the project-needed initial capital is deducted from the equivalent earnings. Equation (19) is expressed NPV:

$$\mathrm{NPV} = -C_0 + \sum_{i=1}^{N} \frac{C_\mathrm{i}}{(1+r)^\mathrm{i}} \tag{19}$$

where C_i is devoted to the i-th period (i-th year or month) is the expected cash flow, C_0 is the initial investment cost, i is the number of periods of project plant life (years or months), and r is the discount rate. The expected cash flow consists of all project expenditures and incomes during the plant life. In this evaluation technique, the project is evaluated as acceptable, profitable, and economical whenever the NPV of a project is positive, while the project is considered as non-profitable and unacceptable if the NPV is negative.

In this technique, through the discounted project income to the investment amount, the discount rate is obtained. The

internal rate of return (IRR), which is considered the discount rate, equals the present value of project income to the present value of its costs, which makes the NPV of all cash flows from a particular project equal to zero. Thus, IRR is calculated through the following relation:

$$\mathrm{NPV} = 0 \Rightarrow \mathrm{NPV} = -C_0 + \sum_{i=1}^{N} \frac{C_\mathrm{i}}{(1+\mathrm{IRR})^\mathrm{i}} \tag{20}$$

According to the investigation, the project is considered as profitable if the project IRR is more than the interest rate of investment. Moreover, the plan will be evaluated as non-economical, if it is less.

Payback period

An investment method for the payback period is employed, which expresses the period of time taken by the investment to recover the principal or initial investment. Thus, Eqs. (21) and (22) are utilized for this purpose. n is the period that the overall initial investment of the project returns to the investors and obtains from the following relations. In other words, a more economical project which attracts to investors' attention has less n index.

$$-C_0 + \sum_{i=1}^{N} (\mathrm{CF})_\mathrm{i} = 0 \tag{21}$$

$$n = \frac{C_0}{\mathrm{CF}} \tag{22}$$

herein CF is the equivalent annual cash flow, and $(\mathrm{CF})_\mathrm{i}$ is the i-th period cash flow. According to the assumptions in Table 5, using the DCF technique and designing a cost–benefit analysis (CBA) model [47], the following results are obtained. In a cold climate in Iran, the NPV for the air–PCM heat exchanger is 1483.36 dollars, and an IRR of 19% is calculated. It should be noted that, after several melting/solidification cycles, the nanoparticles may sediment in the PCM, which is not considered in the economic assumptions. According to Table 6, in the ninth year of exploitation, the air–PCM heat exchanger will return the whole invested capital. In a cold climate, the total rate of return (NPV/I) using the heat exchanger is around 57%. This demonstrates that the project will return 57 cents per one dollar of investment.

Table 6 Economic results of the air–PCM heat exchanger in the Iran's cold climate

Capital expenditures/$	NPV/$	IRR/%	NPV/*I*	(NPV/*I*)/*n*	Payback period (month)
1400	1000	19	0.57	0.032	107

In addition, the annual rate of return ((NPV/*I*)/*n*) for the system is 3.2%.

Conclusions

In this study, the effect of dispersing nanomaterial of multi-wall carbon nanotubes (MWCNT) in a phase change material (PCM) was evaluated. To this end, an air–PCM heat exchanger that could be applied in free cooling of buildings was designed and fabricated. Five similar encapsulations containing PCM were put inside the heat exchanger so that the air can flew through it. The main points are summarized here:

- As the inlet temperature increases, both the efficiencies (energy and exergy) increase during the charging process so that the maximum values are obtained for $T_\mathrm{in} = 29$ °C. Also, both the efficiencies (energy and exergy) increase, as the inlet temperature decreases during the discharging process so that the maximum values are calculated for $T_\mathrm{in} = 13$ °C.
- At a constant inlet temperature, the case of NPCM 0.5 mass% shows the highest efficiencies (energy and exergy) among all cases during the charging and discharging processes. This is due to adding nanoparticles, which leads to improve the heat transfer characteristics.
- The maximum energy efficiency values are 21.33 and 11.44% during the charging and discharging periods, respectively. In addition, the maximum exergy efficiency values are 11.03 and 5.8% during the charging and discharging processes, respectively.
- Exergetic efficiency is always lower than energetic efficiency during charging and discharging periods. This is because the irreversibilities are considered in exergy analysis.
- In outdoor analysis for NPCM 0.5 mass% under three consecutive winter days, it was found that the thermal energy obtained from NPCM 0.5 mass% encapsulations changed with weather conditions. The maximum thermal energy values that charged into and discharged from the encapsulations were 67.1 and − 89.6 W, respectively.
- During three consecutive days, the output energy and exergy changed according to the variations in the sensible and latent heat of NPCM. The maximum values of output energy and exergy were about 325 and 24 kJ, respectively.
- In the ninth year of exploitation, the air–PCM heat exchanger will return the whole invested capital expenditures.
- The project will return 57 cents per one dollar of investment. In addition, the annual rate of return ((NPV/*I*)/*n*) for the current system was 3.2%.

Acknowledgements This research did not receive any specific Grant from funding agencies in the public, commercial, or not-for-profit sectors.

Funding No funding was received to assist with the preparation of this manuscript.

Declarations

Conflict of interest The authors have no competing interests to declare that are relevant to the content of this article.

References

1. Tyagi VV, Pandey AK, Buddhi D, Tyagi SK. Exergy and energy analyses of two different types of PCM based thermal management systems for space air conditioning applications. Energy Convers Manag. 2013;69:1–8. https://doi.org/10.1016/j.enconman.2012.12.028.
2. Dastmalchi M, Boyaghchi FA. Exergy and economic analyses of nanoparticle-enriched phase change material in an air heat exchanger for cooling of residential buildings. J Energy Storage. 2020;32:101705. https://doi.org/10.1016/j.est.2020.101705.
3. Sharma RK, Ganesan P, Tyagi VV, Metselaar HSC, Sandaran SC. Thermal properties and heat storage analysis of palmitic acid-TiO_2 composite as nano-enhanced organic phase change material (NEOPCM). Appl Therm Eng. 2016;99:1254–62. https://doi.org/10.1016/j.applthermaleng.2016.01.130.
4. Eisapour M, Eisapour AH, Hosseini MJ, Talebizadehsardari P. Exergy and energy analysis of wavy tubes photovoltaic-thermal systems using microencapsulated PCM nano-slurry coolant fluid. Appl Energy. 2020;266:114849. https://doi.org/10.1016/j.apenergy.2020.114849.
5. Khan MMA, Saidur R, Al-Sulaiman FA. A review for phase change materials (PCMs) in solar absorption refrigeration systems. Renew Sustain Energy Rev. 2017;76:105–37. https://doi.org/10.1016/j.rser.2017.03.070.
6. Chopra K, Tyagi VV, Pandey AK, Sharma RK, Sari A. PCM integrated glass in glass tube solar collector for low and medium temperature applications: thermodynamic & techno-economic approach. Energy. 2020;198:117238. https://doi.org/10.1016/j.energy.2020.117238.
7. Farzanehnia A, Khatibi M, Sardarabadi M, Passandideh-Fard M. Experimental investigation of multiwall carbon nanotube/paraffin based heat sink for electronic device thermal management. Energy Convers Manag. 2019;179:314–25. https://doi.org/10.1016/j.enconman.2018.10.037.
8. Liao X, Liu Y, Ren J, Guan L, Sang X, Wang B, et al. Investigation of a double-PCM-based thermoelectric energy-harvesting device using temperature fluctuations in an ambient environment. Energy. 2020;202:117724. https://doi.org/10.1016/j.energy.2020.117724.
9. Pakrouh R, Hosseini MJ, Ranjbar AA, Bahrampoury R. A numerical method for PCM-based pin fin heat sinks optimization. Energy Convers Manag. 2015;103:542–52. https://doi.org/10.1016/j.enconman.2015.07.003.
10. Younsi Z, Naji H. Numerical simulation and thermal performance of hybrid brick walls embedding a phase change material for passive building applications. J Therm Anal Calorim. 2020;140(3):965–78. https://doi.org/10.1007/s10973-019-08950-x.
11. Beemkumar N, Yuvarajan D, Arulprakasajothi M, Elangovan K, Arunkumar T. Control of room temperature fluctuations in the building by incorporating PCM in the roof. J Therm Anal Calorim. 2021;143(4):3039–46. https://doi.org/10.1007/s10973-019-09226-0.
12. Tunçbilek E, Arıcı M, Bouadila S, Wonorahardjo S. Seasonal and annual performance analysis of PCM-integrated building brick under the climatic conditions of Marmara region. J Therm Anal Calorim. 2020;141(1):613–24. https://doi.org/10.1007/s10973-020-09320-8.
13. Sari A, Sadi M, Shafiei Sabet G, Mohammadiun M, Mohammadiun H. Experimental analysis and exergetic assessment of the solar air collector with delta winglet vortex generators and baffles. J Therm Anal Calorim. 2021;145(3):867–85. https://doi.org/10.1007/s10973-020-10298-6.
14. Pandey AK, Hossain MS, Tyagi VV, Abd Rahim N, Selvaraj JAL, Sari A. Novel approaches and recent developments on potential applications of phase change materials in solar energy. Renew Sustain Energy Rev. 2018;82:281–323. https://doi.org/10.1016/j.rser.2017.09.043.
15. Kasaeian A, Bahrami L, Pourfayaz F, Khodabandeh E, Yan W-M. Experimental studies on the applications of PCMs and nano-PCMs in buildings: a critical review. Energy Build. 2017;154:96–112. https://doi.org/10.1016/j.enbuild.2017.08.037.
16. Wu S, Zhu D, Zhang X, Huang J. Preparation and melting/freezing characteristics of Cu/paraffin nanofluid as phase-change material (PCM). Energy Fuels. 2010;24(3):1894–8. https://doi.org/10.1021/ef9013967.
17. Mishra AK, Lahiri BB, Philip J. Carbon black nano particle loaded lauric acid-based form-stable phase change material with enhanced thermal conductivity and photo-thermal conversion for thermal energy storage. Energy. 2020;191:116572. https://doi.org/10.1016/j.energy.2019.116572.
18. Kabeel AE, Sathyamurthy R, Manokar AM, Sharshir SW, Essa FA, Elshiekh AH. Experimental study on tubular solar still using Graphene Oxide Nano particles in Phase Change Material (NPCM's) for fresh water production. J Energy Storage. 2020;28:101204. https://doi.org/10.1016/j.est.2020.101204.
19. Rathore PKS, Shukla SK. Improvement in thermal properties of PCM/Expanded vermiculite/expanded graphite shape stabilized composite PCM for building energy applications. Renew Energy. 2021;176:295–304. https://doi.org/10.1016/j.renene.2021.05.068.
20. Zeinelabdein R, Omer S, Gan G. Critical review of latent heat storage systems for free cooling in buildings. Renew Sustain Energy Rev. 2018;82:2843–68. https://doi.org/10.1016/j.rser.2017.10.046.
21. Guelpa E, Verda V. Thermal energy storage in district heating and cooling systems: a review. Appl Energy. 2019;252:13474.
22. Zhou D, Zhao CY, Tian Y. Review on thermal energy storage with phase change materials (PCMs) in building applications. Appl Energy. 2012;92:593–605. https://doi.org/10.1016/j.apenergy.2011.08.025.
23. Li S-F, Liu Z-h, Wang X-J. A comprehensive review on positive cold energy storage technologies and applications in air conditioning with phase change materials. Appl Energy. 2019;255:113667. https://doi.org/10.1016/j.apenergy.2019.113667.
24. Heier J, Bales C, Martin V. Combining thermal energy storage with buildings—a review. Renew Sustain Energy Rev. 2015;42:1305–25. https://doi.org/10.1016/j.rser.2014.11.031.
25. Mosaffa AH, Infante Ferreira CA, Talati F, Rosen MA. Thermal performance of a multiple PCM thermal storage unit for free cooling. Energy Convers Manag. 2013;67:1–7. https://doi.org/10.1016/j.enconman.2012.10.018.
26. Alazwari MA, Abu-Hamdeh NH, Khoshaim A, Ashour AI, Nusier OK, Karimipour A. Effects of examine the phase change material through applying the solar collectors: exergy analysis of an air handling unit equipped with the heat recovery unit. J Energy Storage. 2021;41:103002. https://doi.org/10.1016/j.est.2021.103002.

27. Song J, Sobhani B. Energy and exergy performance of an integrated desiccant cooling system with photovoltaic/thermal using phase change material and maisotsenko cooler. J Energy Storage. 2020;32:101698. https://doi.org/10.1016/j.est.2020.101698.
28. Nikkerdar F, Rahimi M, Ranjbar AA, Pakrouh R, Bahrampoury R. Solar assisted thermal storage system for free heating applications in moderate climates: a case study. Energy. 2021;220:119781. https://doi.org/10.1016/j.energy.2021.119781.
29. Yadav C, Sahoo RR. Exergy and energy comparison of organic phase change materials based thermal energy storage system integrated with engine exhaust. J Energy Storage. 2019;24:100773. https://doi.org/10.1016/j.est.2019.100773.
30. Mosaffa AH, Garousi Farshi L, Infante Ferreira CA, Rosen MA. Energy and exergy evaluation of a multiple-PCM thermal storage unit for free cooling applications. Renew Energy. 2014;68:452–8. https://doi.org/10.1016/j.renene.2014.02.025.
31. Nie B, She X, Yu Q, Zou B, Zhao Y, Li Y, et al. Experimental study of charging a compact PCM energy storage device for transport application with dynamic exergy analysis. Energy Convers Manag. 2019;196:536–44. https://doi.org/10.1016/j.enconman.2019.06.032.
32. Nie B, She X, Zou B, Li Y, Li Y, Ding Y. Discharging performance enhancement of a phase change material based thermal energy storage device for transport air-conditioning applications. Appl Therm Eng. 2020;165:114582. https://doi.org/10.1016/j.applthermaleng.2019.114582.
33. Akbari AD, Talati F, Mahmoudi SMS. New solution method for latent energy storage and thermoeconomic optimization for an air conditioning system. Int J Refrig. 2020;109:12–24. https://doi.org/10.1016/j.ijrefrig.2019.09.012.
34. Tyagi VV, Pandey AK, Buddhi D, Kothari R. Thermal performance assessment of encapsulated PCM based thermal management system to reduce peak energy demand in buildings. Energy Build. 2016;117:44–52. https://doi.org/10.1016/j.enbuild.2016.01.042.
35. Kazemi M, Kianifar A, Niazmand H. Nanoparticle loading effect on the performance of the paraffin thermal energy storage material for building applications. J Therm Anal Calorim. 2020;139(6):3769–75. https://doi.org/10.1007/s10973-019-08647-1.
36. Kazemi M, Kianifar A, Niazmand H. A lab-scale study on thermal performance enhancement of phase change material containing multi-wall carbon nanotubes for buildings free-cooling. Sustain Energy Technol Assess. 2022;50:101813. https://doi.org/10.1016/j.seta.2021.101813.
37. https://www.rubitherm.eu/en/productcategory/organische-pcm-rt.
38. Sivashankar M, Selvam C, Manikandan S, Harish S. Performance improvement in concentrated photovoltaics using nano-enhanced phase change material with graphene nanoplatelets. Energy. 2020;208:118408. https://doi.org/10.1016/j.energy.2020.118408.
39. Zhu N, Wang S, Ma Z, Sun Y. Energy performance and optimal control of air-conditioned buildings with envelopes enhanced by phase change materials. Energy Convers Manag. 2011;52(10):3197–205. https://doi.org/10.1016/j.enconman.2011.05.011.
40. Kuznik F, Virgone J, Roux J-J. Energetic efficiency of room wall containing PCM wallboard: a full-scale experimental investigation. Energy Build. 2008;40(2):148–56. https://doi.org/10.1016/j.enbuild.2007.01.022.
41. Siva Reddy V, Kaushik SC, Tyagi SK. Exergetic analysis of solar concentrator aided natural gas fired combined cycle power plant. Renew Energy. 2012;39(1):114–25. https://doi.org/10.1016/j.renene.2011.07.031.
42. Öztürk HH. Experimental evaluation of energy and exergy efficiency of a seasonal latent heat storage system for greenhouse heating. Energy Convers Manag. 2005;46(9):1523–42. https://doi.org/10.1016/j.enconman.2004.07.001.
43. Ezan MA, Ozdogan M, Gunerhan H, Erek A, Hepbasli A. Energetic and exergetic analysis and assessment of a thermal energy storage (TES) unit for building applications. Energy Build. 2010;42(10):1896–901. https://doi.org/10.1016/j.enbuild.2010.05.025.
44. Kousksou T, Strub F, Castaing Lasvignottes J, Jamil A, Bédécarrats JP. Second law analysis of latent thermal storage for solar system. Sol Energy Mater Sol Cells. 2007;91(14):1275–81. https://doi.org/10.1016/j.solmat.2007.04.029.
45. Tyagi VV, Pandey AK, Giridhar G, Bandyopadhyay B, Park SR, Tyagi SK. Comparative study based on exergy analysis of solar air heater collector using thermal energy storage. Int J Energy Res. 2012;36(6):724–36. https://doi.org/10.1002/er.1827.
46. Pandey AK, Tyagi VV, Park SR, Tyagi SK. Comparative experimental study of solar cookers using exergy analysis. J Therm Anal Calorim. 2012;109(1):425–31. https://doi.org/10.1007/s10973-011-1501-1.
47. Sokhansefat T, Kasaeian A, Rahmani K, Heidari AH, Aghakhani F, Mahian O. Thermoeconomic and environmental analysis of solar flat plate and evacuated tube collectors in cold climatic conditions. Renew Energy. 2018;115:501–8. https://doi.org/10.1016/j.renene.2017.08.057.